Anisotropic straining of graphene using micropatterned SiN membranes

Francesca F. Settembrini, Francesco Colangelo, Alessandro Pitanti, Vaidotas Miseikis, Camilla Coletti, Guido Menichetti, Renato Colle, Giuseppe Grosso, Alessandro Tredicucci, and Stefano Roddaro

Citation: APL Mater. **4**, 116107 (2016); doi: 10.1063/1.4967937
View online: http://dx.doi.org/10.1063/1.4967937
View Table of Contents: http://aip.scitation.org/toc/apm/4/11
Published by the American Institute of Physics

Anisotropic straining of graphene using micropatterned SiN membranes

Francesca F. Settembrini,[1] Francesco Colangelo,[1,2,a] Alessandro Pitanti,[1,b] Vaidotas Miseikis,[3,4] Camilla Coletti,[3,4] Guido Menichetti,[5,1] Renato Colle,[6,5] Giuseppe Grosso,[5,1] Alessandro Tredicucci,[5,1,2] and Stefano Roddaro[1]
[1]*NEST, Istituto Nanoscienze-CNR and Scuola Normale Superiore, I-56126 Pisa, Italy*
[2]*Fondazione Bruno Kessler (FBK), Via Sommarive 18, 38123 Povo, Trento, Italy*
[3]*Center for Nanotechnology Innovation @NEST, Istituto Italiano di Tecnologia, Piazza San Silvestro 12, 56127 Pisa, Italy*
[4]*Graphene Labs, Istituto Italiano di Tecnologia, Via Morego 30, I-16163 Genova, Italy*
[5]*Dipartimento di Fisica "E. Fermi", Università di Pisa, Largo Pontecorvo 3, I-56127 Pisa, Italy*
[6]*DICAM, University of Bologna, Via Terracini 28, I-40136 Bologna, Italy*

(Received 1 July 2016; accepted 28 October 2016; published online 17 November 2016)

We use micro-Raman spectroscopy to study strain in free-standing graphene monolayers anchored to SiN holes of non-circular geometry. We show that a uniform differential pressure load yields measurable deviations from hydrostatic strain, conventionally observed in radially symmetric microbubbles. A pressure load of 1 bar yields a top hydrostatic strain of $\approx 0.7\%$ and a $G_{\pm}$ splitting of 10 cm^{-1} in graphene clamped to elliptical boundaries with axes 40 and 20 μm, in good agreement with the calculated anisotropy $\Delta\varepsilon \approx 0.6\%$ and consistently with recent reports on Grüneisen parameters. The implementation of arbitrary strain configurations by designing suitable boundary clamping conditions is discussed. © *2016 Author(s). All article content, except where otherwise noted, is licensed under a Creative Commons Attribution (CC BY) license (http://creativecommons.org/licenses/by/4.0/).* [http://dx.doi.org/10.1063/1.4967937]

Graphene displays a range of remarkable properties that have catalyzed—since its discovery in 2004[1]—an impressive interest in the scientific community.[2] Its unique electronic behavior stems from the hexagonal honeycomb structure of the carbon lattice, which forces low-energy conducting electrons to assume linear dispersions that mimic massless relativistic fermions.[3] In addition, graphene displays an unusual mechanical strength and strains up to 10% can be applied to it without damaging appreciably its structure.[4] This factor, combined with its intrinsic two-dimensional nature, opens unique perspectives for the investigation of strain engineering[5–7] and for the development of novel device concepts.[8] In fact, it has been predicted,[7,9] and in part experimentally demonstrated,[10,11] that mechanical deformations in graphene can be used to tailor its electron properties. As a particularly inspiring possibility, it is known that a suitable deformation of the honeycomb lattice can be equivalent to the application of a pseudomagnetic field.[6,12]

Achieving a controlled strain profile in graphene poses non-trivial technical challenges and various alternative approaches have been explored during recent years. Hydrostatic configurations were obtained and studied using circular holes and a uniform differential pressure load,[13–15] and the impact of strain was studied by micro-Raman spectroscopy.[16–18] In this device architecture, local strain was also induced or measured taking advantage of scanning probe techniques.[19,20] Differently, uniform biaxial strain configurations could be induced by taking advantage of piezoelectric effects in the substrate[21] and by using pressure transmitting media.[22] Concerning uniaxial strain, various studies have demonstrated the possibility to anisotropically deform graphene deposited on non-flat substrates,[23] on polydimethylsiloxane (PDMS)[24] or on similar stretchable substrates.[25,26] An

[a]Electronic mail: francesco.colangelo1@sns.it
[b]Electronic mail: alessandro.pitanti@sns.it

 © Author(s) 2016

alternative promising approach consists in anchoring graphene layers to micro-electromechanical actuators.[27] More elaborated strain profiles, in particular those giving rise to a pseudomagnetic field, have been hard to demonstrate so far. Interesting experimental evidence has been put forward in the context of random nanobubbles[10] and fascinating results have been obtained in deformed artificial honeycomb structures mimicking the behavior of graphene.[11] In practice, the achievement of custom strain profiles has generally proved to be rather elusive.

In the present work, we demonstrate that markedly non-isotropic strain profiles can be obtained in free-standing graphene membranes that are clamped on an edge that is not radially symmetric and are subject to a vertical uniform load using a pressure difference between the two opposite faces of the graphene flake. In particular, we show that loaded elliptical membranes display Raman features that demonstrate the presence of an anisotropic component in the induced strain profile, in good agreement with what is expected with the studied geometry. The possibility to achieve custom strain profiles by choosing a suitable graphene clamping geometry is discussed.

Figure 1 shows the device architecture and setup adopted for this work. Free-standing graphene areas of various shapes and dimensions were obtained using micropatterned SiN membranes as the mechanical support for the graphene layer. Starting from a Si wafer doubly coated in "pre-stressed" 300 nm of Si_3N_4, a combination of dry and wet etching protocols (see the supplementary material for further details) was adopted to obtain suspended $500 \times 500\ \mu m^2$ Si_3N_4 membranes with through holes of various geometries. In the present study, we investigated a set of elliptical holes with various major (a) and minor (b) axes: $a \times b = 5\ \mu m \times 10\ \mu m$, $10\ \mu m \times 20\ \mu m$, and $20\ \mu m \times 40\ \mu m$. Circular holes were also investigated, as reported in the literature.[17,28] Large-scale monocrystalline graphene flakes used in the present work were obtained by CVD growth on Cu[29] and transferred on the Si_3N_4/Si chips using a standard "bubbling transfer" technique.[30] As sketched in Fig. 1(a), a differential pressure ΔP is applied orthogonally to the free-standing graphene region thanks to a 2 mm-thick polydimethylsiloxane (PDMS) coupling layer placed on top of a modified microscope slide. As a result, the top side of the free-standing graphene region is subject to ambient pressure (conventionally $P_0 = 1$ bar) while the bottom space can be partially or completely evacuated with a scroll pump. Static vacuum tests were performed to verify the stability of ΔP, which was found to

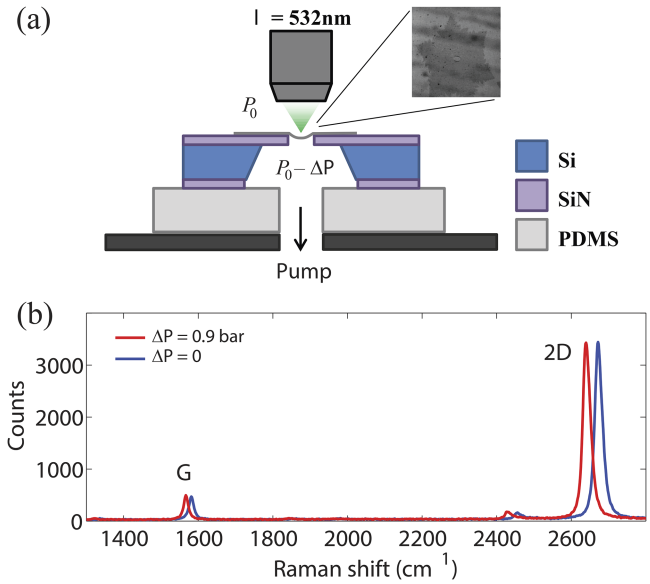

FIG. 1. Straining graphene with a differential pressure load. (a) Sketch of the device architecture. Monolayer CVD graphene is transferred on a patterned SiN membrane. The bottom of the chip is coupled to a vacuum chamber using a polydimethylsiloxane layer, providing a sealing between the two. Deformed graphene is investigated by micro-Raman spectroscopy as a function of the applied differential pressure ΔP with respect to the reference pressure P_0. Right picture: optical image of one of the CVD monocrystals deposited on the patterned Si_3N_4. (b) Raman spectrum measured at $\Delta P = 0$ (blue curve) and $\Delta P = 0.9$ bar (red curve) for an elliptical SiN membrane with axes $20\ \mu m$ and $10\ \mu m$.

decay over a time scale of various hours; this ensures pressure values measured by the gauge are meaningful. Maps were always performed under active pumping conditions, at $\Delta P = 1$ bar.

Local graphene deformation is investigated by micro-Raman spectroscopy, using an *inVia* confocal system by Renishaw equipped with a polarized $\lambda = 532$ nm laser source. Raman signal was collected through a 50× objective with N.A. = 0.75 and analyzed by 1800 grooves/mm grating. Light collection was not polarized, except for a minor polarization selectivity intrinsic in our single-grating monochromator. Raman maps were collected using a laser power of 1 mW to minimize the impact of local heating. Laser polarization was always set along the ellipse minor axis. In Fig. 1(b) we report the measured Raman spectra collected at the center of a 10 μm × 20 μm elliptical graphene region, for $\Delta P = 0$ (blue curve) and $\Delta P = 0.9$ bar (red curve); as expected, the G and $2D$ Raman peaks are significantly red shifted by strain in the suspended graphene region. Importantly, the modification of the Raman spectra was always found to be completely reversible upon removal of the pressure load. In addition, as visible from the maps of Fig. 2, no significant Raman shift was observed in the regions where graphene is supported by the SiN, even in the proximity of the hole. This proves that no measurable adjustment or sliding of graphene occurs during our experiments.

The most evident impact of deformation upon ΔP is visible in Fig. 2, where we compare the map of the $2D$ peak Raman shift ω_{2D} for $\Delta P = 0$ (Fig. 2(a)) and $\Delta P = 1$ bar (Fig. 2(b)). For symmetry reason, its center frequency is sensitive to the hydrostatic component of the strain tensor ε_{ij}, which we name $\bar{\varepsilon} = (\varepsilon_{xx} + \varepsilon_{yy})/2$. Experimentally, the $2D$ peak displays a maximal red shift at the center of the suspended region, similar to what was reported for inflated circular graphene membranes.[17] The quantitative evolution of the shift versus ΔP is highlighted in Fig. 2(c) where we report ω_{2D} measured at the maximal shift region at the center of the ellipse. The phononic mode giving rise to the higher order $2D$ peak is sketched in Fig. 2(d). Raman shifts at various pressure loads are compared with the adimensional parameter $\eta = (\Delta P/P_0)^{2/3}$, where $P_0 = 1$ bar; all the components of the strain tensor ε_{ij} are in fact expected to scale linearly with η, as highlighted for specific cases in the recent literature.[16]

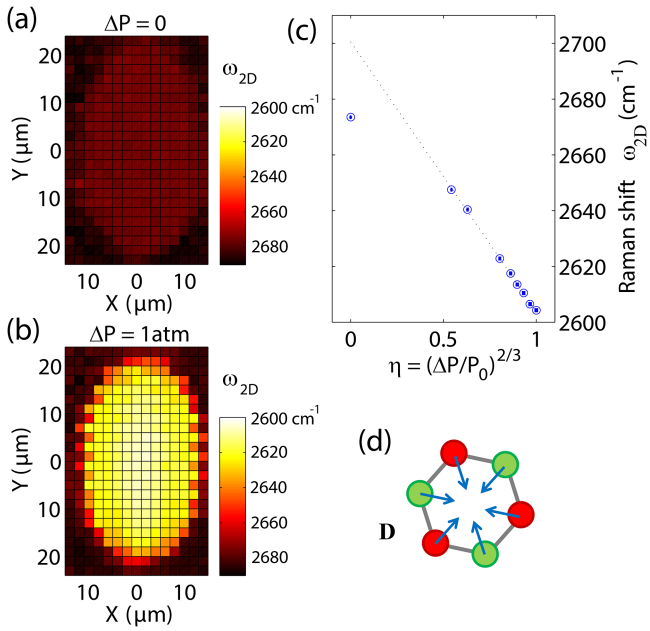

FIG. 2. Impact of strain on the 2D peak. (a) Map of the position of the 2D peak for $\Delta P = 0$; the peak position is mostly uniform with a slight red shift over the suspended region (see discussion in the main text). (b) The application of a differential pressure $\Delta P = 1$ bar leads to a dome-shaped shift, which is maximal at the center of the membrane. As further argued based on data presented in Fig. 3, this effect can be explained as the consequence of a hydrostatic strain $\bar{\varepsilon}$ in the elliptical hole. (c) Evolution of the Raman shift as a function of the parameter $\eta = (\Delta P/P_0)^{2/3}$, which is proportional to $\bar{\varepsilon}$. A linear regression of the observed Raman shifts (excluding the value at $\eta = 0$) and a comparison with numerical estimates of the strain yield a Grüneisen parameter consistent with most recent results reported in the literature. (d) Sketch of the D mode in graphene, whose second order causes the 2D Raman resonance.

The validity of such a scaling law is also formally demonstrated, for a general clamping geometry, in the supplementary material. The overall dependence of ω_{2D} as a function of ΔP and of the position on the ellipse is found to be largely consistent with reports on the simpler case of radially symmetric graphene clamping and with the most recent estimates of the Grüneisen parameters.[16,25,31] We also note that, consistently with reported data,[16] the value of ω_{2D} for $\Delta P \approx 0$ is found to display a further surprising red shift. This effect was attributed to uncertainties in the exact determination of ΔP. We believe that an additional reason for the shift is possibly related to graphene adhesion on the vertical sidewalls of the SiN hole, which is known to occur in this kind of graphene drums[16] and could be relevant in the low-ΔP regime. The verification of this hypothesis will likely require a combined Raman and atomic force microscopy study at low pressure loads, which goes beyond the scope of the present work. Further details regarding the numerical calculation of the ε_{ij} tensor as a function of ΔP and scaling rules are reported in the supplementary material.

While hydrostatic deformations explain well the coarse evolution of the Raman spectra, the strain profiles in our elliptically clamped graphene membranes are expected to display a marked deviation from a uniform strain configuration and a larger strain can be expected along the shorter axis of the ellipse. More in general, the anisotropic component of the strain field can be expressed through the invariant

$$\Delta\varepsilon = \sqrt{(\varepsilon_{xx} - \varepsilon_{yy})^2 + 4\varepsilon_{xy}^2} \tag{1}$$

corresponding to the difference between two eigenvalues of the strain tensor $\varepsilon = \bar{\varepsilon} \pm \Delta\varepsilon/2$. It is well known[31] that strain anisotropy, when sufficiently large, can be detected in Raman spectroscopy as a splitting of the degenerate phononic modes $G_{\pm}$. In Fig. 3 we report a detailed study of the Raman spectrum of the G peak region as a function of ΔP. Data reported in Fig. 3 refer to the largest explored Si_3N_4 elliptical $20 \times 40\ \mu m^2$ hole; larger suspended areas in fact correspond—for a given value of ΔP—to a larger anisotropic strain $\Delta\varepsilon$.

A first rough analysis was performed by fitting the Raman data with a single Lorentzian peak. As visible in Fig. 3(a), the resulting map of the Raman shift ω_G at $\Delta P = 1$ bar is found to be consistent with the ω_{2D} map reported in Fig. 2(a). For comparison, we report in Fig. 3(b) the map of $\bar{\varepsilon}$ calculated for the same pressure load. A top hydrostatic strain of 0.68% is expected, in agreement with the observed red shift of the G peak and known values of the corresponding Grüneisen parameter (see the supplementary material for further details). As argued in the following, on the other hand, hydrostatic

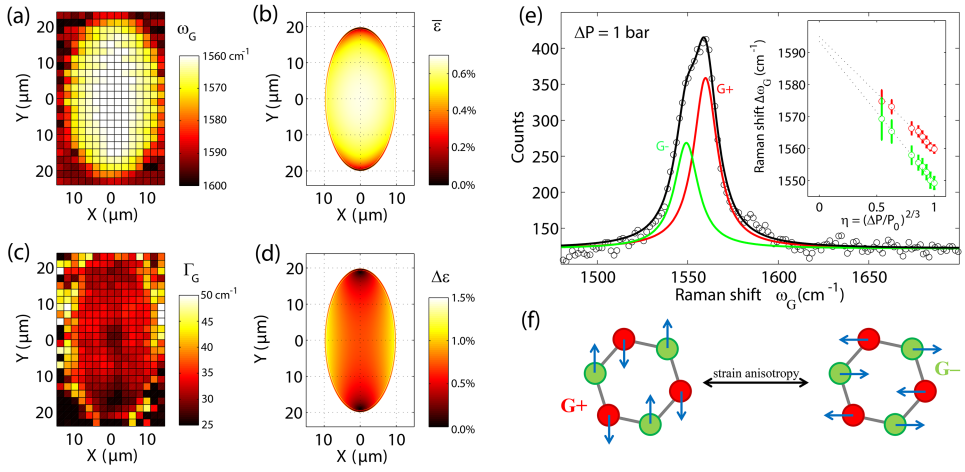

FIG. 3. Strain-induced shift and splitting of the G peak. (a) Map of the Raman shift ω_G obtained by fitting the G peak with a single Lorentzian curve. (b) Simulated average strain map $\bar{\varepsilon} = (\varepsilon_{xx} + \varepsilon_{yy})/2$ at $\Delta P = 1$ bar. (c) Map of the peak broadening Γ_G obtained by fitting the G peak with a single Lorentzian curve. (d) Simulated strain anisotropy map $\Delta\varepsilon = \sqrt{(\varepsilon_{xx} - \varepsilon_{yy})^2 + 4\varepsilon_{xy}^2}$ at $\Delta P = 1$ bar. (e) Multipeak fit of the G peak at $\Delta P = 1$ bar measured at the center of the elliptical hole. The resulting positions of the G_+ (red curve and markers) and G_- (green curve and markers) peak versus ΔP are reported in the inset along with a weighted linear fit. (f) Sketch of the G_+ and G_- modes in the presence of an arbitrary anisotropic strain.

strain is not sufficient to satisfactorily describe the evolution of the G peak as a function of the pressure load. Indeed, a non-trivial broadening is visible in Fig. 3(c), where we report the FWHM Γ_G resulting from the same fitting procedure. The observed broadening displays a peculiar "saddle point" spatial evolution, with large Γ_G values close to the central part of the ellipse, while a significantly smaller effect is observed at the top and bottom apexes. Remarkably, a very similar pattern is visible in Fig. 3(d), displaying the calculated $\Delta\varepsilon$ for the same clamping geometry, at $\Delta P = 1$ bar. This suggests that, beyond mechanisms highlighted in recent works,[16] broadening in our experiment is also in part connected to strain anisotropy.

A more detailed investigation of the broadening mechanism was performed through the analysis of the G peak measured at the center of the elliptical hole, which represents a good trade-off between the expected value of $\Delta\varepsilon$ and the minimization of the impact of the borders of the Si_3N_4 hole. In this position, numerical estimates indicate that a top anisotropic strain component $\Delta\varepsilon = 0.64\%$ can be expected. The Raman spectrum in the G peak region for $\Delta P = 1$ bar is reported in Fig. 3(e); the peak displays a lineshape which is clearly consistent with the superposition of two nearby Lorentzian peaks, which we interpret as corresponding to the G_+ and G_- modes in uniaxially strained graphene (see Fig. 3(f)). A similar analysis (see the supplementary material for further information concerning the fitting procedure) was performed for various values of ΔP and the resulting peak positions are reported in the inset to Fig. 3(e). Two divergent peaks are obtained with a top splitting of about 10 cm^{-1}, which is in very good agreement[31] with what is expected for an anisotropy $\Delta\varepsilon = 0.64\%$. A weighted linear regression of the two peak positions $\omega_{G_\pm}$ yields two remarkably linear trends in η that converge almost exactly for $\Delta P = 0$, as expected. It is important to note that, since light collection in our experiment is *not* polarized, both G_+ and G_- are expected to be visible. In fact, only a minor amplitude difference is observed, as a likely consequence of the residual polarization sensitivity of our single-grating monochromator. Finally, we note that no evidence of a clear splitting of the $2D$ peak could be detected in the current experiments, differently from what was reported in other works.[32] Since the $2D$ splitting strongly depends on the strain direction, this behavior could be linked to the orientation of the studied flakes with respect to the ellipse axes.

Our work demonstrates that non-trivial strain profiles can be obtained in Si_3N_4 holes with an elliptical shape and that a sizable anisotropic component in the graphene strain can be obtained. Similarly, we expect that more in general clamping geometries can be used to design even more advanced non-uniform and non-isotropic strain profiles, taking advantage of a relatively robust implementation with no free graphene edges. The relevant case of triaxial strain, which however also requires a correct crystalline orientation to give rise to a pseudo magnetic field, is reported in the supplementary material. In view of the possibility to impact the electronic states via the engineering of custom strain profiles, the observed $G_\pm$ splitting phenomenology has also been compared with a first-principle calculation on an atomistic model system mimicking the experimental setup. To this end, we have simulated an unstrained suspended graphene layer with an elliptic-shape depression (see the inset of Fig. 4). To reproduce the experimental configuration, we have fixed the position of the carbon atoms external to the ellipse to a "zero" height, as it happens for graphene on Si_3N_4 substrate, and the effect of the vertical load has been reproduced by fixing the two carbon atoms at the center of the ellipse (blue dots in the inset) at a lower vertical position and leaving all the other carbon atoms in the ellipse free to relax in order to reach the minimum energy structure. The simulation has been performed on a 7.4 Å × 12.8 Å ellipse containing a total of 22 carbon atoms. The Raman spectra of the system have been calculated by means of density functional perturbation theory[33] as implemented in QUANTUM-ESPRESSO code,[34] with local density approximation and norm-conserving pseudopotential for the carbon atoms.[35] We used a plane wave expansion up to 80 Ry cutoff and $4 \times 4 \times 1$ Monkhorst-Pack mesh[36] for the sampling of Brillouin zone. The ellipse depression was created in the central part of a 5×5 graphene supercell with the minimum energy configuration lattice parameter $a_0 = 12.24$ Å.

In the absence of strain, the frequency of the degenerate G phononic mode is $\omega_G = 1607.5$ cm^{-1}. For $\Delta P \neq 0$, the value of the effective strain along the ellipse axes has been estimated from the depth of the two central carbon atoms, δ and the length of the principal axes of the ellipse, a and b; e.g., for the major axis we have $\varepsilon_a \sim (2L - a)/a$ where $L \sim \sqrt{(a/2)^2 + \delta^2}$ is the profile length for the depression

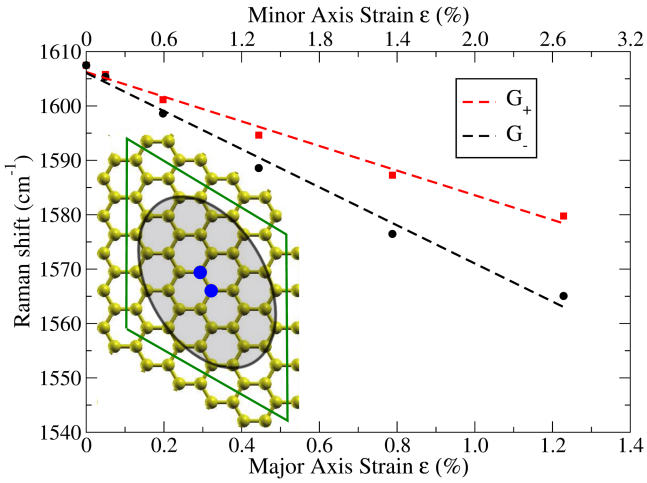

FIG. 4. Position of the $G_{\pm}$ peak as function of the major axis strain. The slope of the Raman shifts is $\partial\omega_{G_-}/\partial\varepsilon_a \sim -35\ \mathrm{cm}^{-1}/\%$ for G_- and $\partial\omega_{G_+}/\partial\varepsilon_a \sim -23\ \mathrm{cm}^{-1}/\%$ for G_+. The inset shows the simulation cell (green) containing the ellipse. The lowest fixed carbon atoms are indicated in blue.

along the *a* direction; the same holds for the minor axis. The results of the calculation are shown in Fig. 4; the asymmetry of the strain due to the elliptical geometry of the depression is responsible of an averaged splitting of the *G* peak mode that is found to be of the same order of magnitude as the one experimentally induced by uniaxial strain on the graphene layer.[25]

In conclusion, we have provided evidence of an incipient splitting of the *G* mode in free-standing graphene regions clamped to elliptical holes in Si_3N_4 and subject to a uniform differential pressure load. Our results indicate a promising route to induce custom strain profiles, which can be controlled by the applied pressure load and *designed* according to the chosen geometry of the supporting Si_3N_4 frame. We also highlight that our experiment has been performed using large scale CVD monocrystalline graphene flakes, thus providing a route for scalable strain-engineered graphene devices. Finally, we would like to stress that present results have been obtained using a vacuum chamber to induce a maximal load $\Delta P = 1$ bar. A recent report[16] demonstrates that using pressurized gas as a load it is possible to reach $\Delta P = 14$ bar, potentially leading to significantly increased achievable strain magnitude (about a factor six larger strain can be expected) and/or to less stringent limits on the minimal area of the Si_3N_4 holes.

See the supplementary material for more details about sample fabrication, numerical calculations, demonstration of the scaling law, and Raman measurements. An example of a hole geometry which induces a triaxial strain profile with the related pseudo-magnetic field is also given.

This work was supported by the EC under the Graphene Flagship Program (Contract No. CNECT-ICT-604391) and by the ERC advanced grant SoulMan (No. G.A. 321122). The authors acknowledge the "IT center" of the University of Pisa for the computational support and the allocation of computer resources from the CINECA, ISCRA C Project Nos. HP10C6H6O1 and HP10CAI9PV. F.C., A.P., and S.R. thank S. Gröblacher and R. Norte for their help in the initial development of this experiment. S.R. acknowledges the support of the CNR through the bilateral CNR-RFBR projects. F.C. acknowledges support from Fondazione Silvio Tronchetti Provera.

[1] K. Novoselov, D. Jiang, F. Schedin, T. Booth, V. Khotkevich, S. Morozov, and A. Geim, "Two-dimensional atomic crystals," Proc. Natl. Acad. Sci. U. S. A. **102**, 10451–10453 (2005).
[2] A. K. Geim and K. S. Novoselov, "The rise of graphene," Nat. Mater. **6**, 183–191 (2007).
[3] A. C. Neto, F. Guinea, N. Peres, K. S. Novoselov, and A. K. Geim, "The electronic properties of graphene," Rev. Mod. Phys. **81**, 109 (2009).
[4] C. Lee, X. Wei, J. W. Kysar, and J. Hone, "Measurement of the elastic properties and intrinsic strength of monolayer graphene," Science **321**, 385–388 (2008).
[5] V. M. Pereira and A. C. Neto, "Strain engineering of graphene electronic structure," Phys. Rev. Lett. **103**, 046801 (2009).
[6] T. Low and F. Guinea, "Strain-induced pseudomagnetic field for novel graphene electronics," Nano Lett. **10**, 3551–3554 (2010).

[7] F. Guinea, "Strain engineering in graphene," Solid State Commun. **152**, 1437–1441 (2012).
[8] Z. Qi, D. Bahamon, V. M. Pereira, H. S. Park, D. Campbell, and A. C. Neto, "Resonant tunneling in graphene pseudomagnetic quantum dots," Nano Lett. **13**, 2692–2697 (2013).
[9] A. K. Geim, "Graphene: Status and prospects," Science **324**, 1530–1534 (2009).
[10] N. Levy, S. Burke, K. Meaker, M. Panlasigui, A. Zettl, F. Guinea, A. C. Neto, and M. Crommie, "Strain-induced pseudo–magnetic fields greater than 300 tesla in graphene nanobubbles," Science **329**, 544–547 (2010).
[11] M. Polini, F. Guinea, M. Lewenstein, H. C. Manoharan, and V. Pellegrini, "Artificial honeycomb lattices for electrons, atoms and photons," Nat. Nanotechnol. **8**, 625–633 (2013).
[12] F. Guinea, M. Katsnelson, and A. Geim, "Energy gaps and a zero-field quantum hall effect in graphene by strain engineering," Nat. Phys. **6**, 30–33 (2010).
[13] J. S. Bunch, S. S. Verbridge, J. S. Alden, A. M. Van Der Zande, J. M. Parpia, H. G. Craighead, and P. L. McEuen, "Impermeable atomic membranes from graphene sheets," Nano Lett. **8**, 2458–2462 (2008).
[14] A. L. Kitt, Z. Qi, S. Remi, H. S. Park, A. K. Swan, and B. B. Goldberg, "How graphene slides: Measurement and theory of strain-dependent frictional forces between graphene and SiO_2," Nano Lett. **13**, 2605–2610 (2013).
[15] S. P. Koenig, N. G. Boddeti, M. L. Dunn, and J. S. Bunch, "Ultrastrong adhesion of graphene membranes," Nat. Nanotechnol. **6**, 543–546 (2011).
[16] Y. Shin, M. Lozada-Hidalgo, J. L. Sambricio, I. V. Grigorieva, A. K. Geim, and C. Casiraghi, "Raman spectroscopy of highly pressurized graphene membranes," Appl. Phys. Lett. **108**, 221907 (2016).
[17] J. Zabel, R. R. Nair, A. Ott, T. Georgiou, A. K. Geim, K. S. Novoselov, and C. Casiraghi, "Raman spectroscopy of graphene and bilayer under biaxial strain: Bubbles and balloons," Nano Lett. **12**, 617–621 (2012).
[18] J.-U. Lee, D. Yoon, and H. Cheong, "Estimation of youngs modulus of graphene by raman spectroscopy," Nano Lett. **12**, 4444–4448 (2012).
[19] S. Zhu, Y. Huang, N. N. Klimov, D. B. Newell, N. B. Zhitenev, J. A. Stroscio, S. D. Solares, and T. Li, "Pseudomagnetic fields in a locally strained graphene drumhead," Phys. Rev. B **90**, 075426 (2014).
[20] R. Beams, L. G. Cançado, A. Jorio, A. N. Vamivakas, and L. Novotny, "Tip-enhanced raman mapping of local strain in graphene," Nanotechnology **26**, 175702 (2015).
[21] W. Jie, Y. Y. Hui, Y. Zhang, S. P. Lau, and J. Hao, "Effects of controllable biaxial strain on the raman spectra of monolayer graphene prepared by chemical vapor deposition," Appl. Phys. Lett. **102**, 223112 (2013).
[22] K. Filintoglou, N. Papadopoulos, J. Arvanitidis, D. Christofilos, O. Frank, M. Kalbac, J. Parthenios, G. Kalosakas, C. Galiotis, and K. Papagelis, "Raman spectroscopy of graphene at high pressure: Effects of the substrate and the pressure transmitting media," Phys. Rev. B **88**, 045418 (2013).
[23] C. Metzger, S. Rémi, M. Liu, S. V. Kusminskiy, A. H. Castro Neto, A. K. Swan, and B. B. Goldberg, "Biaxial strain in graphene adhered to shallow depressions," Nano Lett. **10**, 6–10 (2009).
[24] M. Huang, H. Yan, C. Chen, D. Song, T. F. Heinz, and J. Hone, "Phonon softening and crystallographic orientation of strained graphene studied by raman spectroscopy," Proc. Natl. Acad. Sci. U. S. A. **106**, 7304–7308 (2009).
[25] T. Mohiuddin, A. Lombardo, R. Nair, A. Bonetti, G. Savini, R. Jalil, N. Bonini, D. Basko, C. Galiotis, N. Marzari *et al.*, "Uniaxial strain in graphene by raman spectroscopy: G peak splitting, Grüneisen parameters, and sample orientation," Phys. Rev. B **79**, 205433 (2009).
[26] Z. H. Ni, T. Yu, Y. H. Lu, Y. Y. Wang, Y. P. Feng, and Z. X. Shen, "Uniaxial strain on graphene: Raman spectroscopy study and band-gap opening," ACS Nano **2**, 2301–2305 (2008).
[27] H. H. Perez Garza, E. W. Kievit, G. F. Schneider, and U. Staufer, "Controlled, reversible, and nondestructive generation of uniaxial extreme strains (>10%) in graphene," Nano Lett. **14**, 4107–4113 (2014).
[28] C. Si, Z. Sun, and F. Liu, "Strain engineering of graphene: A review," Nanoscale **8**, 3207 (2016).
[29] V. Miseikis, D. Convertino, N. Mishra, M. Gemmi, T. Mashoff, S. Heun, N. Haghighian, F. Bisio, M. Canepa, V. Piazza *et al.*, "Rapid cvd growth of millimetre-sized single crystal graphene using a cold-wall reactor," 2D Mater. **2**, 014006 (2015).
[30] L. Gao, W. Ren, H. Xu, L. Jin, Z. Wang, T. Ma, L.-P. Ma, Z. Zhang, Q. Fu, L.-M. Peng *et al.*, "Repeated growth and bubbling transfer of graphene with millimetre-size single-crystal grains using platinum," Nat. Commun. **3**, 699 (2012).
[31] Y. Cheng, Z. Zhu, G. Huang, and U. Schwingenschlögl, "Grüneisen parameter of the G mode of strained monolayer graphene," Phys. Rev. B **83**, 115449 (2011).
[32] M. Mohr, J. Maultzsch, and C. Thomsen, "Splitting of the raman 2 d band of graphene subjected to strain," Phys. Rev. B **82**, 201409 (2010).
[33] S. Baroni, S. De Gironcoli, A. Dal Corso, and P. Giannozzi, "Phonons and related crystal properties from density-functional perturbation theory," Rev. Mod. Phys. **73**, 515 (2001).
[34] P. Giannozzi, S. Baroni, N. Bonini, M. Calandra, R. Car, C. Cavazzoni, D. Ceresoli, G. L. Chiarotti, M. Cococcioni, I. Dabo *et al.*, "Quantum espresso: A modular and open-source software project for quantum simulations of materials," J. Phys.: Condens. Matter **21**, 395502 (2009).
[35] N. Troullier and J. L. Martins, "Efficient pseudopotentials for plane-wave calculations," Phys. Rev. B **43**, 1993 (1991).
[36] H. J. Monkhorst and J. D. Pack, "Special points for brillouin-zone integrations," Phys. Rev. B **13**, 5188 (1976).